Free-Rocket Trajectory Errors from Plume-Induced Loading during Tube Launch

W.H. Appich Jr.* and D.E. Tipping†
Martin Marietta Aerospace, Orlando, Fla.

Aerodynamic loads induced on the body of a free rocket during launch from a tube have been investigated by using a cold-gas (N_2) static test facility. The rocket had four wrap-around fins, forward bore riders, aft spin rail guides, and a seven-orifice nozzle configuration. Circumferential pressure measurements at various body stations were used to obtain resultant differential pressure distributions. Body pressures were affected by chamber pressure (thrust), gravity drop, longitudinal position of the rocket in the tube, and nozzle orientation. The differential pressure distributions were incorporated into a six-degree-of-freedom computer simulation to estimate the error contribution, using the error budget technique. The plume-induced loading on the rocket afterbody was shown to be a significant source of trajectory error.

Nomenclature

CEP = circular error of probability
D = diameter of nozzle
L = longitudinal distance of pressure orifice from exit of launch tube
P = pressure
X = longitudinal distance from launch tube exit to center nozzle exit plane
Z = vertical distance from centerline of launch tube
α = angle between tangent to jet boundary and nozzle axis
θ = nozzle half-angle
ϕ = circumferential angle on rocket model, clockwise from top as viewed from base

Subscripts

A = atmospheric
E = exit
M = matching condition
N = equivalent single nozzle used as reference dimension
0 = plenum chamber
R = orifice location
res = resultant
S = seven-nozzle configuration
SB = rocket model body static

Introduction

THE tube-launched free rocket fired as a barrage weapon has been under increasing scrutiny since it offers lower cost, rapid fire, and increased effectiveness if the required accuracy can be obtained. It is essential, for good accuracy, to limit the error sources created during launch. One method used to minimize mallaunch effects is to release the rocket from front and rear supports simultaneously to avoid "tipoff." Generally, this requires a launch tube larger in cross section at the front than at the rear. The forward part of the rocket in such nontipoff launch tubes is supported by sabots or bore riders (as in the present study). Spin rails constrict the flow in the rear half of the tube.

In the design under consideration, the rocket is launched under full thrust, flying free off the rails. Packaging constraints dictate a relatively low nozzle exit-to-throat area ratio. Consequently, the plume is highly underexpanded and impinges on the tube wall at a steep angle. The pressure rise associated with that turn and the impingement on the spin rails tend to cause some of the flow in the mixing region to be deflected forward into the annular area between the rocket body and the tube. The maximum cross-sectional area of the tube additionally limits the plume expansion, resulting in static pressures of up to 20.7 psia at the maximum thrust level. If choked flow occurs, it would contribute to the forward motion of the gases.

This forward flow, or blow-by, tends to be nonuniform and, coupled with rocket body protuberances, can cause lateral loading on the rocket. Preliminary analyses showed that the corresponding moment can be large and have a significant effect on the total accuracy. Consequently, an experimental program was conducted to evaluate the magnitude of this error source. The major objectives of this program were to measure 1) pressure distributions on the afterbody of a rocket model inside a launch tube, in order to calculate possible induced effects, and 2) pitot pressure in the body-tube annulus, to evaluate the direction and velocity of the flow.

An existing high-pressure nitrogen facility was selected to provide the rocket plume simulation because of cost, safety, technical risk, and schedule. This facility can supply measured mass flow rates of up to 30 lb/sec at regulated pressures to 3000 psia. Simulations of rocket-motor exhaust properties using cold gasses have been extensively researched and applied.[1] Static testing was chosen because greater testing efficiencies can be obtained in parametric investigations and because prior static and dynamic rocket firings have shown qualitative agreement in the measurement of tube-wall static pressures.[1] In dynamic rocket firings, the exhaust gas velocity is typically greater than the maximum rocket velocity in the launch tube by at least an order of magnitude; hence, the exhaust flow is assumed to be quasisteady. The assumption of steady flow and the approximation of hot-gas properties by cold gas were considered acceptable technical risks. However, tube-wall pressure measurements were not expected to equal the rocket body pressures because protuberances on the rocket and the launch tube geometry will increase the nonuniformity of the annular velocity profile. This consideration dictates use of instrumentation on the rocket body.

Model Description

The experimental arrangement is shown in Fig. 1, which also defines the axis system. Linear measurements were set up to ±0.01 in. in positioning the rocket model in the launch

Received Jan. 17, 1977; presented as Paper 77-81 at the AIAA 15th Aerospace Sciences Meeting, Jan. 24–26, 1977; revision received June 16, 1977.

Index categories: LV/M Simulation; Jets, Wakes, and Viscid-Inviscid Flow Interactions.

*Senior Aerophysics Engineer. Member AIAA.
†Principal Staff Engineer. Associate Fellow AIAA.

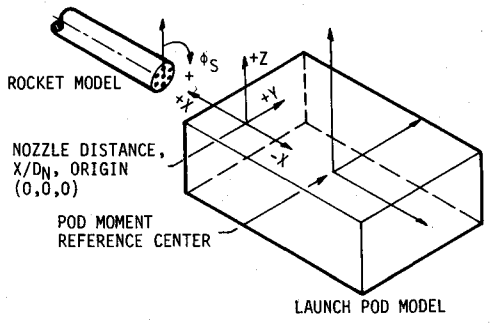

Fig. 1 Rocket model, launch pod, and axis system.

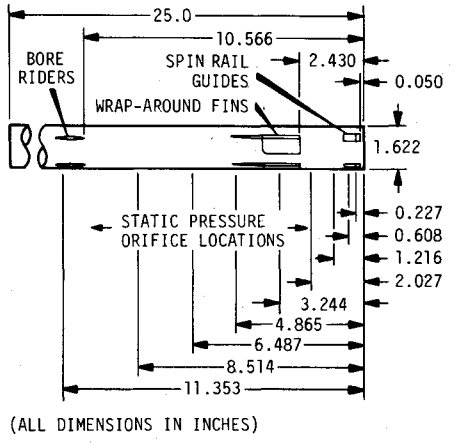

Fig. 2 Rocket model geometry and pressure orifice locations.

tube. A 2-mW helium-neon laser was mounted aft of the launch pod, and a front-surfaced mirror was positioned on the rocket nozzle centerline to provide a visible light path for angular alignment of the rocket body and launch tube within ±0.1 deg.

Model Geometry

An outer diameter of 1.622 in. for the rocket afterbody was selected to facilitate adequate modeling detail without developing excessive thrust and launch pod loads. External model protuberances consisted of four wrap-around fins, forward bore riders, and spin rail guides near the base (Fig. 2). The rocket had a length-to-diameter ratio of 13.44. The nitrogen gas used for the exhaust plume simulation was supplied through a mounting hub at the forward end of the rocket body. The total length of the rocket model and hub was 25.0 in. (15.41 diameters). Geometric details of the bore riders, wrap-around fins, and spin rail guides are shown in Fig. 3. The tube-to-body diameter ratio was 1.28. Local obstructions (blockage) in the body-tube annulus produced by the bore riders, fins, and rail guides totaled 0.7, 11.4, and 6.0%, respectively. In the rear half of the launch tube, the spin rails reduced the local cross-sectional area by 2.2%. The spin rail geometry is shown in Fig. 4.

Test Instrumentation

The nitrogen supply line pressure and mass flow were measured during each run, and the model plenum chamber pressure was controlled by a manual regulator. Two solenoid-driven 48-port scanning valves equipped with ±5-psid transducers were used to measure the rocket pressures. Static pressures were obtained for as many as 12 circumferential orifice locations for each longitudinal station on the rocket model. The orifice stations are shown in Fig. 2. During the first half of its travel through the launch tube, tipoff of the rocket was constrained by the bore riders and spin rails; consequently, the orifice locations extended only seven body diameters forward of the model base.

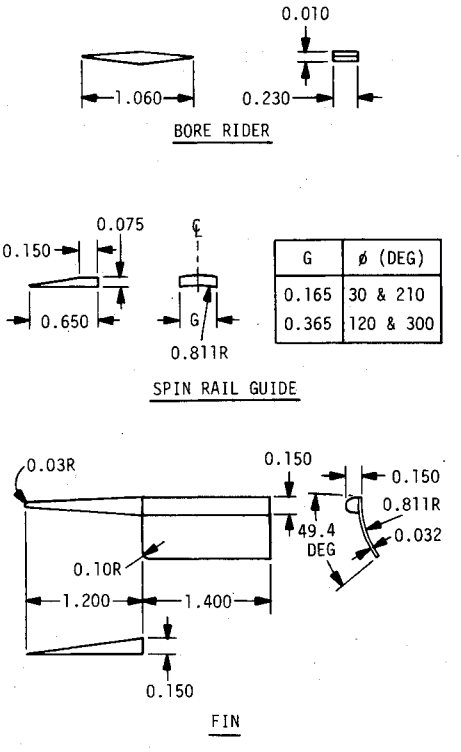

Fig. 3 Bore rider, spin rail guide, and fin details.

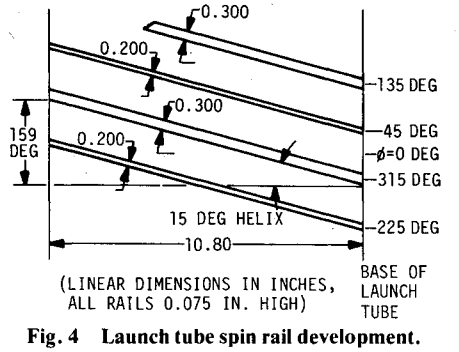

Fig. 4 Launch tube spin rail development.

Pitot pressure tubes were mounted facing forward and aft at two peripheral body locations ($\phi = 60$ and 240 deg) near the base of the rocket model. The forward- and aft-facing pitot tubes were approximately 0.9 and 0.5 model diameters forward of the base, respectively. These tubes were positioned radially such that their centerlines were at the midpoint of the body-tube annulus. Only two pairs of pitot tubes were used in order to limit their blockage in the body-tube annulus to 0.8%.

A total of seven scanning valve ports were used to sample atmospheric pressure during each test run. The barometric pressure during the tests was 14.74 psia, and the atmospheric pressure obtained by averaging the sampled readings was 14.74±0.05 psia. All test data were recorded on oscillographs.

Propulsion Characteristics

A seven-orifice nozzle design was used to promote rapid plume decay,[3] thus reducing the external impingement loads on the launch pod. The nozzle geometry is illustrated in Fig. 5. During earlier tests comparing exhaust plume characteristics, a single nozzle of equivalent geometry and cold-gas performance had been used as a baseline. The single-nozzle exit diameter D_N of 1.271 in. was chosen as the reference dimension for all plume measurements and model positioning

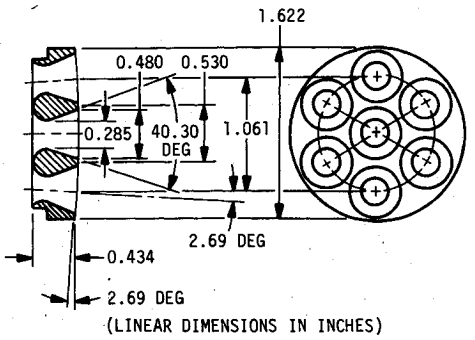

Fig. 5 Rocket nozzle geometry.

for both the single and multiple nozzle tests. Nozzle geometry and operating conditions were established by two criteria:

1) Pressure distributions on a rocket afterbody inside a launch tube would be affected primarily by nozzle exit pressure and the angle between the jet boundary and the nozzle axis (initial turning angle).

2) External plume-induced loads on the launch pod would be represented best by developing a specified motor thrust of 1000 lb.

It was decided that a single, seven-orifice nozzle design could satisfy both of the preceding requirements by using two chamber pressures, 1890 psia to match exit pressure and 1530 psia to develop the 1000 lb thrust. Test runs also were made at two lower chamber pressures to investigate the effects of thrust.

An expansion half-angle of 20.1 deg was required to match the initial jet boundary angle for the rocket afterbody pressure test (matched exit pressure). This initial angle was not considered to be of primary importance for the launch pod test, where the maximum loads would be expected to occur when the exhaust plume was fully developed. A specific heat ratio of 1.4 was used, and a total temperature of 520°R was assumed for the nitrogen gas. Propulsion parameters for the multiple nozzle design are summarized in Table 1.

Test Program and Results

Plenum chamber pressure effects, simulated gravity drop Z/D_N, nozzle orientation angle ϕ_S, and longitudinal position in the launch tube were investigated. Representative circumferential and longitudinal pressure distributions are presented for each of these parameters.

Chamber Pressure

Typical circumferential pressure variations are shown in Fig. 6 for four nozzle plenum chamber pressures at $X/D_N = -8.22$ (just forward of the spin rails in the launch tube). The rocket was positioned concentrically in the tube ($Z/D_N = 0$) with three of the seven nozzles in a vertical row ($\phi_S = 0$ deg). At the lowest chamber pressure, the body circumferential pressure distribution is essentially uniform and approximately 0.97 psi below ambient (14.74 psia). The pressure on the upper part of the body becomes slightly less than on the lower part at a chamber pressure of 1020 psia. At the two higher chamber pressures, body pressure distributions are significantly asymmetrical, the maximum variations being slightly more than 0.5 psi. These data were obtained at a longitudinal orifice station, $L/D_N = -7.26$, midway from the trailing edges of the fins to the nozzle exit plane and are representative of the lateral loading induced on the body aft of the fin leading edges. Circumferential pressure distributions forward of the fins, but aft of the tube exit, are not presented herein. However, in this region, the pressure distributions become relatively uniform. Outside the tube exit, all rocket body pressures are essentially equal to ambient at all test chamber pressures.

Table 1 Cold-gas propulsion characteristics

Parameter	Matched thrust	Matched exit pressure
Nominal thrust, lb	1000	1260
Chamber pressure P_0, psia	1530	1890
Jet boundary angle α, deg	43.2	43.2
Nozzle half-angle ϕ_M required to match α, deg	22.3	20.1
Design nozzle half-angle θ_E, deg	20.1	20.1
Exit static pressure P_E, psia	79	97

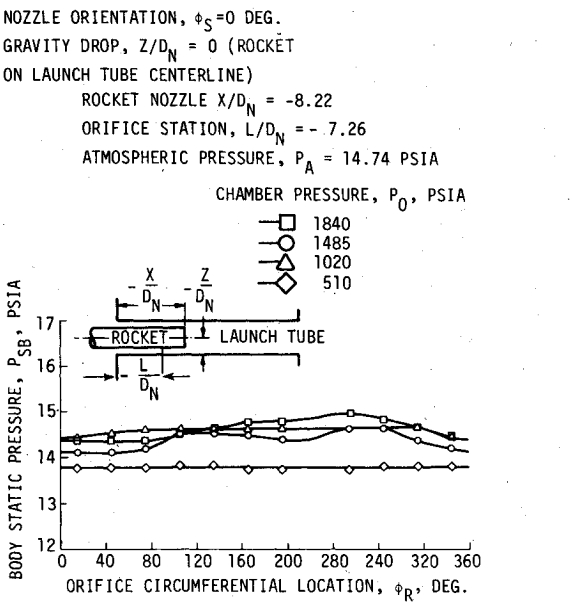

Fig. 6 Effect of chamber pressure on rocket body pressure distribution.

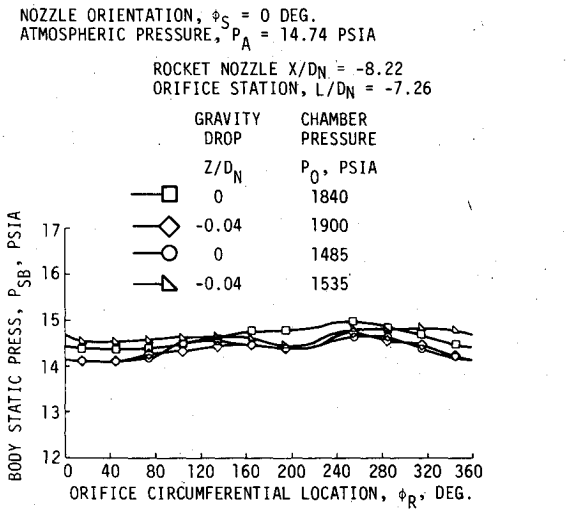

Fig. 7 Effect of simulated gravity drop on rocket body pressure distribution.

Simulated Gravity Drop

Gravity drop was simulated by a downward displacement ($Z/D_N = -0.04$) of the rocket body in the launch tube. The effects of gravity drop on circumferential pressure distributions are presented in Fig. 7 for the same rocket nozzle and orifice stations as in Fig. 6. At chamber pressures approximating matched thrust conditions ($P_0 = 1530$ psia), the rocket body pressures are higher and more uniform with gravity drop than at $Z/D_N = 0$. Gravity drop reduces body pressures at a chamber pressure approximating matched exit

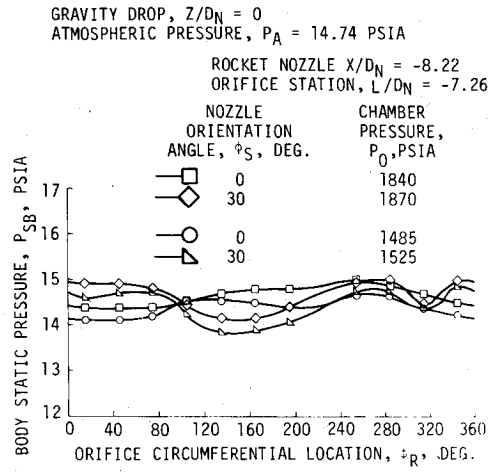

Fig. 8 Effect of nozzle orientation angle on rocket body pressure distribution.

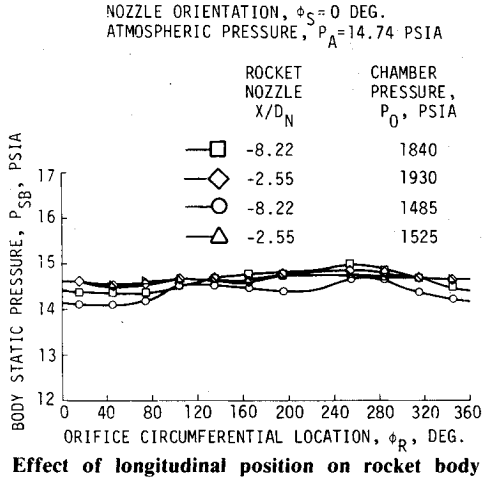

Fig. 9 Effect of longitudinal position on rocket body pressure distribution.

pressure conditions ($P_0 = 1890$ psia). However, the circumferential variations are similar at both Z/D_N values for this chamber pressure.

Nozzle Orientation Angle

Angular position change due to spin was simulated statically by changing the nozzle orientation angle relative to the launch tube. In the model tested, six equally spaced peripheral nozzles surround a centerline nozzle. Circumferential body pressure data are shown in Fig. 8 for nozzle orientation angles of 0 deg (three nozzles in a vertical row) and 30 deg (three nozzles horizontal). For each orientation angle, the circumferential pressure distributions are similar for both chamber pressure levels. Conversely, the 30-deg nozzle orientation angle produces significantly greater circumferential pressure variations at each chamber pressure level. The strong effect of orientation angle is attributed to the change in interaction of the six peripheral nozzle exhaust plumes with the four spin rails and the tube wall.

Longitudinal Position

Rocket model pressure data were obtained at two longitudinal positions in the launch tube with no gravity drop and $\phi_S = 0$ deg. As shown in Fig. 9, moving the model forward from $X/D_N = -8.22$ to $X/D_N = -2.55$ reduces the circumferential pressure variation and minimizes the effect of chamber pressure. These data were measured at the orifice station midway from the fin trailing edges to the nozzle exit plane. At X/D_N values of -8.22 and -2.55, the normalized orifice distances aft of the tube exit are $L/D_N = -7.26$ and

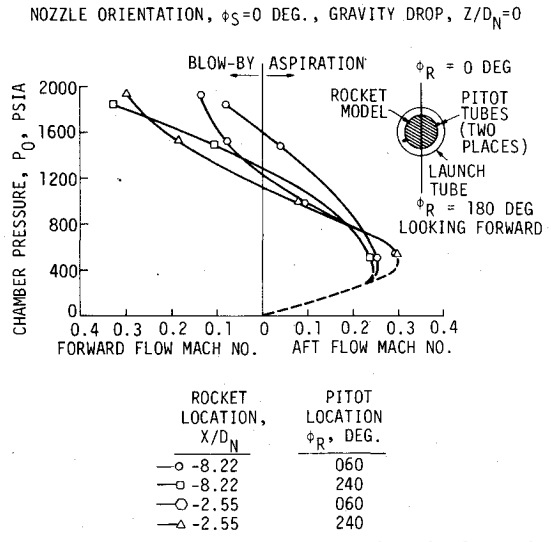

Fig. 10 Effect of chamber pressure on launch tube venting.

-1.59, respectively. The increasing uniformity of the pressure distributions aft of the fins, but near the launch tube exit, is quite similar to the uniformity forward of the fins and approaching the tube exit, which was alluded to in the earlier discussion of chamber pressure. It supports other test results showing that, in close proximity to the spin rails, the nozzle exhaust plumes interact in a highly complex manner, producing asymmetric pressure distributions on the rocket.

Launch Tube Venting

Pitot pressure measurements were made at two circumferential locations to gain insight into the direction and Mach number of the gas relative to the rocket. The pitot tubes, at $\phi = 60$ and 240 deg, were displaced circumferentially from the body protuberances. Longitudinally, the pitot tubes were aft of the trailing edge of the fins and forward of the tip of the spin rail guides. These locations were chosen to obtain pressure measurements for a broad range of model positions in the tube while minimizing the effects of protuberances on these data. As previously mentioned, only two pairs of pitot tubes were used, limiting their blockage to less than 1% of the annular area.

The effect of P_0 on the venting of the gas in the body-tube annulus is presented in Fig. 10. At a chamber pressure of approximately 500 psia, the nozzle acts as an ejector, drawing air aft over the rocket model. The Mach number of the flow is slightly less than 0.3. This aftward flow (aspiration) at low chamber pressure produces relatively uniform circumferential pressures on the rocket body. At some chamber pressure less than 500 psia, the aspiration Mach number begins to decrease toward zero, as indicated by the extrapolated curves in the figure.

Forward flow of the gas over the rocket model (blow-by) is initiated at chamber pressures ranging from 1100 to 1600 psia and increases in Mach number with increase in chamber pressure. At the higher chamber pressures, the expanding nozzle plumes interact with the launch tube wall and rails, creating the blow-by that produces the asymmetric pressure distributions observed near the base of the rocket model. This reversed flow is initiated at the wall of the tube and expands to fill the space between the missile and wall as it proceeds up the tube. The multiple nozzle configuration produces curvature of the flow reversal line on the tube wall, thus complicating the flow. At the higher plenum chamber pressures tested, the total head in the reverse flow was adequate to insure exhausting to atmospheric conditions even though body static pressures could be less than atmospheric (refer to Figs. 5-9). It should be noted that these test results were obtained for a stationary rocket model. The blow-by Mach number relative to a moving

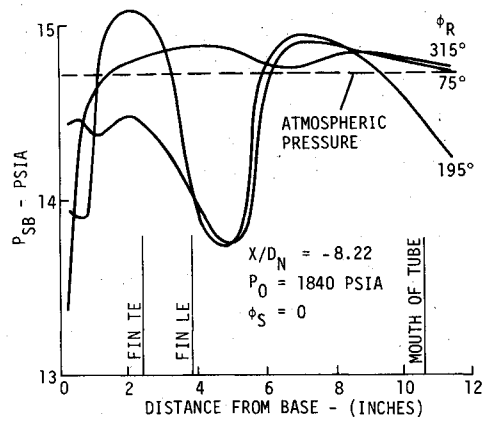

Fig. 11 Longitudinal pressure distribution.

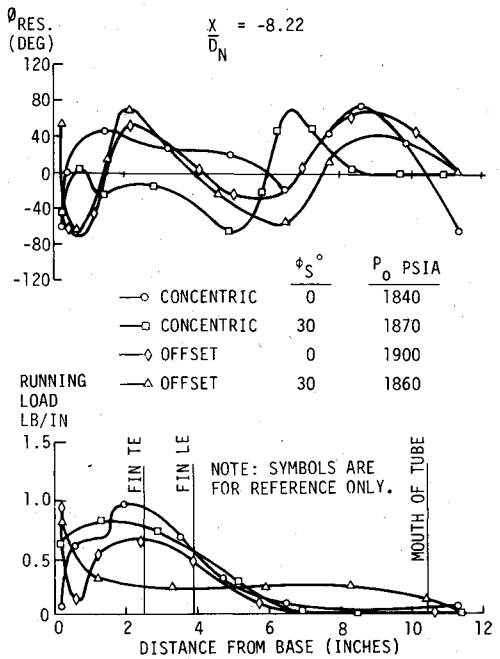

Fig. 12 Effect of gravity drop and nozzle orientation on loading, missile leaving rails.

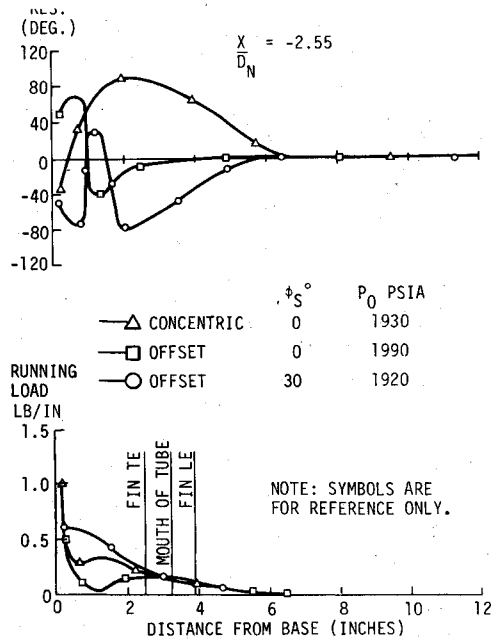

Fig. 13 Effect of gravity drop and nozzle orientation on loading, missile exiting tube.

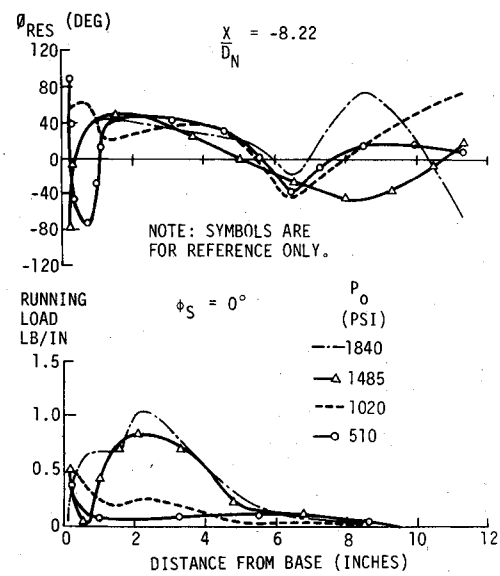

Fig. 14 Effect of chamber pressure on loading.

rocket would be reduced by its forward velocity, and, conversely, the aspiration Mach number would be increased.

Body Loading

In general, higher thrust levels are desirable because the boost action time for a fixed range is reduced, minimizing the time-dependent errors in boost. The high thrust, however, does induce the reverse flow investigated in the tests just described and produces a loading on the rocket when it is free of constraints but still in the tube, which is equivalent to an increased mallaunch rate. The following discussion is limited to the highest thrust level, which corresponds to matched nozzle exit conditions.

Based upon the previous data, it is postulated that a vortex region is established which extends to varying lengths along the body, depending upon the circumferential position. This postulate is consistent with the low pressures (Fig. 11) close to the base. The flow is complicated further by the restrictions of the guides and folded fins shown in Fig. 2. Longitudinal pressure distributions for one rocket location in the tube are given in Fig. 11, which shows varying pressures indicative of mixed flow conditions. The cirucmferential pressure distributions (Figs. 6–8) show similar indications. Since the objective of this test was to obtain the missile body loading, the surface pressure measurements are not adequate to explore the reversed flow completely, and this has not been attempted beyond the obvious observations.

The circumferential pressures were integrated to give the running load on the missile body. This was effected by applying constant pressure, as measured, over each sector, resolving vertically and horizontally, and obtaining the resultant. The orientation followed from the arctangent of the ratio of the components. The results are shown in Figs. 12–14. Some effects of the geometry are clear. The folded fins provide the largest blockage in the annular passage and would, by that restriction, tend to smooth out the flow. Consequently, the largest change in running load would be expected to be at the expansion past the fin leading edge while in the tube. A significant drop in the loading is evident past the leading edge in Fig. 12. When the rocket moves up the tube until the leading edge is clear, the sudden expansion in the annulus is removed and the loading drops significantly, as shown in Fig. 13.

Test data involving gravity drop show a reduction in loading compared to the concentric case (Figs. 12 and 13).

The circumferential pressure distribution for the gravity drop condition shows reduced pressure where the gap is narrow, the net effect being a reduction in the loading. Rotation of the missile brings the multiple nozzle into a different alignment with the spin rails and alters the flow pattern and the loading, especially near the base.

The angular orientation of the resultant running load shows considerable variation in Figs. 12–14. This variation is not relieved by gravity drop or rocket position in the tube. The process of obtaining this angle makes it very sensitive to small variations in the components of the resultant force; therefore, its direction is considered very uncertain. Some variation is expected, and these results are included in order to illustrate this point. For conservatism, it was decided to use this differential in a single plane. The results presented are directly applicable only to a similar configuration, since changes in relative diameter will alter the plume conditions at the wall. Rocket, nozzle, and tube geometry also affect these conditions. Rocket forward motion also will modify the conditions and, to the first order, one might expect that the resultant loading will vary with the local dynamic pressure based upon the relative velocity of the gas to the rocket.

Effect on Accuracy

The effect of the induced rocket loading in the tube was explored as part of a configuration study of a barrage weapon system for a rocket launched in a ripple-fire mode. The accuracy obtained is the net effect of the errors from launch through boost, ballistic flight, and munition dispensing and dispersion. The error budget technique, frequently used in preliminary design, was employed by using a six-degree-of-freedom simulation of a spinning rocket with 18 precision error and 6 bias error sources. This is an adequate procedure for evaluating differing design concepts and establishing feasibility, but to produce estimates of accuracy in field conditions for a detailed design, it would be necessary to resort to a Monte Carlo analysis. The standard techniques for estimating accuracy are given in Ref. 4; however, these techniques have been modified to account for the effects of highly underexpanded plumes on longitudinal static stability.

It was assumed that the induced loading was random in angular orientation and did not roll with the missile. This was thought to be representative, because the pressure differential would be a function of relative tube and rocket geometry and not appreciably affected by the spin rate. In order to adjust the static test results for rocket motion, the measured loads were reduced by the ratio of the dynamic pressure based upon relative gas velocity to the dynamic pressure based upon measured blow-by. This brought the peak running load down to 0.24 lb/in. (based upon model dimensions). The longitudinal load distribution varies with position in the tube (i.e., with time in the simulation). Data from the two longitudinal stations tested were not sufficient to establish this time variation fully. Therefore, simplified distributions made up of linear elements were assumed, giving zero loading at exit from the tube.

The rocket was simulated with full thrust out of the tube, with the opening of the fin delayed until the rocket cleared the tube and with the tube shielding the rocket in a crosswind. After traveling half its length from rest, the rocket was free of the spin rails. The rocket design was conventional, with a thrust-to-weight ratio of 59 at launch. This level of thrust loading affects the stability, and this interaction was incorporated in the simulation. Reduction of thrust would alleviate the asymmetric body loading at the expense of increasing other errors, and so tradeoffs must be made at the system level.

Table 2 Effect of plume-induced loading on accuracy

Error sources (1σ)		Long range		Intermediate range	
		Down-range, mils	Cross-range, mils	Down-range, mils	Cross-range, mils
Precision					
GSE Elevation	1 mrad	0.21	....	0.52	....
Azimuth and yaw	1 mrad each	....	1.97	....	1.63
Rocket Elevation	1 mrad	0.31	....	0.52	....
Yaw	1 mrad	....	1.70	....	1.29
Mallaunch	17 mrad/sec	1.37	7.50	2.28	4.76
Inert weight	0.4%	3.62	....	1.71	....
Drag	0.5%	3.25	....	2.48	....
Static margin/surface wind	0.2D/16.0 fps	1.25	4.16	0.79	2.66
I_{sp}	0.21%	4.03	....	2.35	....
Propellant weight	0.2%	3.07	....	1.43	....
Thrust	2.0%	2.55	....	1.26	....
Thrust alignment	0.7 mrad	0.93	5.05	1.54	3.21
Thrust offset	0.01 in.	0.17	0.94	0.29	0.60
Principal axis	0.12 mrad	0.61	3.32	1.01	2.11
c.g. offset	0.01 in.	0.17	0.94	0.29	0.60
Fuze time (0.1%) and preset (0.01 sec)	....	0.62	....	0.58	....
Warhead event	0.012 sec	0.06	....	0.12	....
Bias					
Survey azimuth	1 mrad	....	1.0	....	1.0
Launcher Elevation	1 mrad	0.31	....	0.52	....
Azimuth	1 mrad	....	1.0	....	1.0
Ballistic wind	10 fps	2.76	2.30	2.15	1.82
Munition wind	10 fps	0.33	0.34	0.47	0.43
Atmospheric density	0.5%	3.25	....	2.48	....
Totals (1σ)	....	8.91	11.22	6.29	7.41
CEP	....	11.78		8.01	
Plume-induced loading	....	1.68	8.95	2.78	5.76
Totals (revised)	....	9.07	14.35	6.88	9.39
CEP	....	13.70		9.51	

The results of this investigation are incorporated into Table 2, which gives the error budget for two ranges. The budget contains the error sources considered and the magnitude allocated. Remembering that the summing process is root-sum-squares, the plume-induced loading is seen to be very significant, with the effect mainly in the cross-range component. The change in CEP at long range means that the area within which 50% of the munitions fall has increased by 35%, with a corresponding decrease in effectiveness.

Conclusions

Asymmetric body loading on a free rocket during launch has been shown to be a significant error source. Thrust level, orientation of the multiple nozzles, and rocket body position in the launch tube affect the loading. For this particular combination of configuration geometry and test conditions, the following conclusions are drawn:

1) The longitudinal body loading associated with a peak value of 0.24 lb/in. induced by blow-by in the body-tube annulus will increase the CEP by 35% at maximum range.

2) Blow-by is induced at high thrust levels, with limited pitot pressure measurements indicating that the maximum blow-by Mach number is approximately 0.3.

3) At low thrust levels, the body-tube annulus is aspirated, with uniform body pressure resulting.

Other variables, such as tube-to-body diameter ratio and spin rail geometry, can be expected to influence the interaction of the underexpanded nozzle plume with the tube wall, which initiates the blow-by. These considerations imply that in-tube launch conditions should be determined experimentally in order to provide a quantitative input to the acuracy estimate.

References

[1] Hensel, R.W., "A Survey of Recent Developments in Wind Tunnel Testing Techniques at Transonic and Supersonic Speeds," *Journal of Spacecraft and Rockets,* Vol. 1, Sept-Oct. 1964, pp. 449-463.

[2] Bertin, J.J. and Batson, J.L., "Experimentally Determined Rocket-Exhaust Flowfield in a Constrictive Tube Launcher," *Journal of Spacecraft and Rockets,* Vol. 12, Dec. 1975, pp. 771-717.

[3] Appich, W.H. Jr., "Free Rocket Technology Cold Gas Plume Loads and Pressure Data," Martin Marietta Corp., GSR TRP-0097000-001, July 1976.

[4] "Design of Aerodynamically Stabilized Free Rockets," *Engineering Design Handbook,* Headquarters, U.S. Army Materiel Command, AD 840 582, July 1968.